Chemical Sensing with Nanowires

Reginald M. Penner

Departments of Chemistry and Chemical Engineering/Materials Science, University of California, Irvine, California 92697; email: rmpenner@uci.edu

Annu. Rev. Anal. Chem. 2012. 5:461–85

First published online as a Review in Advance on April 9, 2012

The *Annual Review of Analytical Chemistry* is online at anchem.annualreviews.org

This article's doi: 10.1146/annurev-anchem-062011-143007

1936-1327/12/0719-0461$20.00

Keywords

biosensor, transistor, ISFET, PNA, DNA, protein, virus, biomarker, cancer marker

Abstract

Transformational advances in the performance of nanowire-based chemical sensors and biosensors have been achieved over the past two to three years. These advances have arisen from a better understanding of the mechanisms of transduction operating in these devices, innovations in nanowire fabrication, and improved methods for incorporating receptors into or onto nanowires. Nanowire-based biosensors have detected DNA in undiluted physiological saline. For silicon nanowire nucleic acid sensors, higher sensitivities have been obtained by eliminating the passivating oxide layer on the nanowire surface and by substituting uncharged protein nucleic acids for DNA as the capture strands. Biosensors for peptide and protein cancer markers, based on both semiconductor nanowires and nanowires of conductive polymers, have detected these targets at physiologically relevant concentrations in both blood plasma and whole blood. Nanowire chemical sensors have also detected several gases at the parts-per-million level. This review discusses these and other recent advances, concentrating on work published in the past three years.

1. INTRODUCTION

The first research papers describing the use of chemical sensors based on metal and semiconductor nanowires appeared in 2001 (1, 2). A search for the keywords nanowire and sensor within the Web of Science reveals that more than 700 papers on this subject have appeared in the 10 years since then. This expansive landscape has been the subject of several excellent, comprehensive reviews (3–6), so we do not attempt another such review here. Instead, our goal is to identify and describe some key advances that have occurred at the frontier of this fast-moving field over the past three years. We focus on transformational improvements or advances involving (*a*) the performance of nanowire-based sensors, (*b*) sensor fabrication and integration, and (*c*) our understanding of transduction mechanisms for nanowire-based sensors. Biosensors and chemical sensors rely on fundamentally different mechanisms for recognizing and binding target analyte species, so we discuss these two types of sensors separately below.

2. BIOSENSORS

Nanowire field-effect transistors (NWFETs) have dominated work in the area of nanowire-based biosensing since their discovery by Lieber et al. (2) in 2001. The function of these devices is identical to that of the ion-selective field-effect transistors (ISFETs) first described by Bergveld (7, 8) in the early 1970s. With ISFETs, the charge on a chemically modified channel is inferred from measurements of either the conductivity of the channel or its capacitance, and the relationship between the charge, σ_0, and surface potential, Ψ_0, is given by the Grahame equation (9),

$$\sigma_0 = \sqrt{8\varepsilon_w \varepsilon_0 kTC_0}\sinh\left(\frac{e\Psi_0}{2kT}\right), \quad (1)$$

where k is the Boltzmann constant, T is the temperature, e is the elementary charge, ε_0 is the permittivity of free space, ε_w is the dielectric constant of water, and C_0 is the ionic strength of the buffer. In 2002, Manalis et al. (10) first used an ISFET to detect DNA on the basis of its negative charge. Surprisingly, this capability of macroscopic ISFETs was developed at nearly the same time as NWFET biosensors for DNA.

We organize this review of nanowire-based biosensors into two categories according to the method by which the nanowires are prepared. Bottom-up nanowires are synthesized from molecular precursors by use of solution-phase synthetic methods, vapor-liquid-solid (VLS) growth, or other methods. Top-down nanowires are obtained by selectively removing material from macroscopic structures, for example, commercially available silicon-on-insulator (SOI) wafers. Top-down nanowires were discovered first, so research in this area is more mature, and its progress has been thoroughly reviewed (3–6). For this reason, we devote less space to it here and concentrate on especially new and novel work in two categories. Biosensors based on top-down nanowires represent a new paradigm for nanowire sensor fabrication, and so far few overviews of this work have appeared. We devote more space to those biosensors here for this reason.

2.1. Nanowires Fabricated by Bottom-Up Synthesis

Two subcategories of experiments that deserve examination here are (*a*) experiments in which the nanowire biosensor has been liberated from a surface and (*b*) experiments that involve polymer-based nanowire biosensors. Surprising and exciting advances in both types of experiments have occurred over the past two years.

2.1.1. Liberating the nanowire field-effect transistor from the surface. In principle, biosensors based on free-standing nanowires, such as those obtained via solution-based synthetic methods or VLS growth, do not need to be attached to a surface. However, to secure electrical contacts to these minute structures, to simplify the fabrication of microfluidic channels required to deliver analyte molecules to the biosensor, and to provide for a back-gate electrode, attachment of the nanowire to a surface virtually always occurs.

Lieber et al. (11) recently described biosensors based on unsupported, V-shaped NWFETs mounted to atomic force microscopy cantilevers that can be manipulated in three dimensions (**Figure 1*a*,*b***). These intricate, single-crystal NWFETs are obtained by manipulating the growth conditions both to shape the nanowire, by introducing 120° kinks by varying the growth pressure, and to modulate the dopant density. Nanowires are degenerately n^{++} doped, except for short, 200-nm segments, which are selectively doped to much lower extents. In this study (11), only these segments of the longer, V-shaped nanowire functioned as the transistor.

An objective of this study (11) was to probe the electrical activity at the interior of living cardiomyocytes. The concept of using nanowire-based sensors to monitor the electrical activity of single cells is one that Lieber et al. (13) had explored earlier by using arrays of NWFETs patterned onto planar surfaces. In that experiment, the cantilever supporting the NWFET was bent perpendicular to the surface (**Figure 1*c***), enabling it to puncture and penetrate a single cardiomyocyte supported on a second planar surface positioned above the cantilever. The electrical signals measured by this probe depended on the depth to which the probe was inserted into the cell (**Figure 1*c***). The 120-Hz beat pattern in **Figure 1*d*** was observed only at the interior of the cell and emerged only upon insertion of the probe through the cell membrane (11). Clearly, such nanowire-based probes could contribute to future fundamental investigations of cell function.

2.1.2. Polymeric nanowires for biosensing. Most work involving nanowires of conductive polymers, such as polyaniline (PANI), polypyrrole (PPy), polythiophene (PT), and poly(3,4-ethylenedioxythiophene) (PEDOT), has concentrated on applications to gas sensing. We review recent work in that category in Section 3.4, below. Several publications have demonstrated the utility of these polymeric nanomaterials in biosensors, which is an emerging trend in nanowire-based sensing.

In 2005, Myung and coworkers (14) became some of the first investigators to demonstrate the feasibility of biosensing by using single PPy nanowires in which a receptor was entrained during polymerization. In this study, PPy nanowires were electrodeposited within a 100–200-nm-wide channel patterned between two gold (Au) electrical contacts (15, 16). Avidin-conjugated ZnSe/CdSe quantum dots (QDs) within the pyrrole-containing electrodeposition solution were entrained within these PPy nanowires during the electrodeposition process. PPy nanowires containing these avidin-conjugated QDs showed an electrical resistance that increased by 20% to 50% over background in the presence of a biotin-DNA conjugate, which allowed for the detection of 1 nM of this molecule with a good signal-to-noise ratio (14).

This result motivated additional fundamental investigations of PPy nanowires in aqueous ambients in an attempt to understand the extrinsic factors, such as pH and the ionic composition of the solution, that influence the electrical response of these nanowires. In 2010, Mulchandani et al. (17) demonstrated that single PPy nanowires, configured as FETs, show a strong *n*-type gate effect. At gate potentials, V_G negative of the threshold voltage V_{TH}, a strong influence of solution pH on the source-drain current I_{DS}, versus V_G is observed in which I_{DS} increases linearly with increasing pH. No pH response is observed near V_{TH}, and a much weaker and inverted pH response is found for V_G positive of V_{TH}. Importantly, these observations show that application

of a gate voltage can provide for (*a*) enhanced sensitivity of a PPy nanowire to target molecules and (*b*) tunability of the PPy nanowire response (17).

Building on these results, Mulchandani et al. (18) showed in 2009 that covalent attachment chemistries can be used to ensure stable attachment between an antibody to the cancer marker CA-125 and a PPy nanowire. The authors compared the efficacy of glutaraldehyde (GA) and

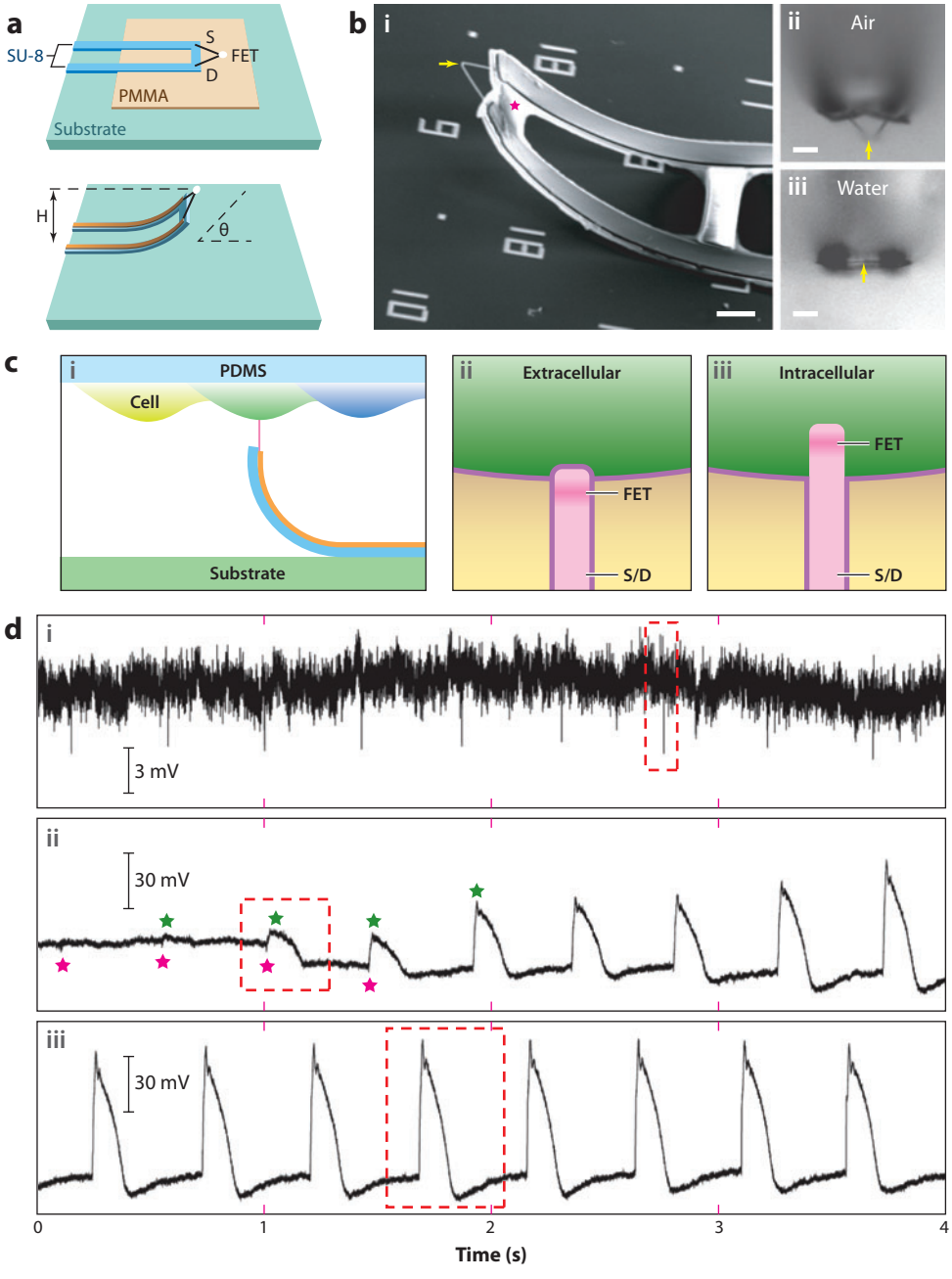

N-(3-dimethylaminopropyl)-*N*′-ethylcarbodiimide hydrochloride (EDC) chemistries; EDC attachment produced higher immobilized antibody concentrations within the PPy nanowire. Following blocking with bovine serum albumin (BSA), these biofunctionalized nanowires detected CA-125 at a decreased electrical conductivity, $\Delta S/S_0 \approx -0.5$, in 1.0 units ml^{-1} in human blood plasma. $\Delta S/S_0$ increased linearly with CA-125 concentration to -0.8 at 1,000 units ml^{-1} (18). The utility of these PPy nanowires in the label-free detection of CA-125 in real human blood plasma represents a significant advance for such biosensors. The mechanism by which bound CA-125 induces a resistance increase of the PPy nanowire is still not understood, however.

These ideas have been extended to PANI nanowires by Yun et al. (19, 20), who recently introduced both antibodies (20) and DNA aptamers (19) into these nanowires by using EDC chemistry. Interestingly, the exposure of functionalized and BSA-blocked PANI nanowires to immunoglobulin G (IgG) induces an increase in the conductivity of the nanowire—an inversion of the response, as compared with the observations of Mulchandani et al. (18). In this case, IgG was detected at 0.030 μg ml^{-1} at $\Delta S/S_0 \approx +2$, whereas myoglobin was detected at 0.008 μg ml^{-1} with a similar conductivity increase (20). Aptamer-biofunctionalized PANI nanowires showed a significantly higher sensitivity—down to 0.56 pg ml^{-1}, which corresponds to ≈3 fM—for the detection of IgG (19). Together with the results of the Myung and Mulchandani groups (14–18) outlined above, these data demonstrate the tremendous potential for biofunctionalized nanowires for label-free detection of proteins and peptides.

Together with Greg Weiss's research group, we (21, 22) have evaluated a biofunctionalization strategy for PEDOT nanowires prepared by lithographically patterned nanowire electrodeposition (LPNE) process (**Figure 2*a***) (23–25). Our approach is characterized by the use of engineered virus particles, instead of antibodies or aptamers, as receptors in our biosensors. With phage-display methods, virus particles can be engineered to display nonnatural peptides on the surface of each virus particle as a C-terminal fusion to most of the coated peptides. From a library of 10^{10} to 10^{11} different peptide epitopes, individual peptide sequences can be identified to strongly and selectively bind virtually any target molecule (26). Previously (26–29), we demonstrated that Au electrode surfaces onto which such virus particles are attached can function as biosensors to detect the binding of target molecules to immobilized virus particles. We have exploited virus particles as receptors in nanowire-based biosensors as follows. Using LPNE, we patterned the electrodeposition of PEDOT nanowires, with typical dimensions of 150 nm (width) × 40 nm (height), onto glass (**Figure 2*b***). When this electrodeposition process was carried out in a solution containing

Figure 1

Three-dimensional kinked nanowire probes. (*a*) Schematics of device fabrication. Patterned poly(methylmethacrylate) (PMMA) and SU-8 microribbons serve as a sacrificial layer and a flexible device support, respectively. The dimensions of the lightly doped *n*-type silicon segment (*white dots*) are ∼80 × 80 × 200 nm^3. H and q are the tip height and orientation, respectively, and S and D designate the built-in source and drain connections to the nanoscale field-effect transistor (FET), respectively. (*b*) (*i*) Scanning electron microscopy and (*ii*,*iii*) bright-field optical microscopy images of an as-made device. The yellow arrow and the pink star mark the nanoscale FET and SU-8, respectively. Panels *ii* and *iii* were recorded in air and water, respectively. Scale bars, 5 mm. (*c*) Electrical recordings from beating cardiomyocytes. (*i*) Schematics of a cellular recording from the cardiomyocyte monolayer on polydimethylsiloxane (PDMS). (*ii*) Extracellular and (*iii*) intracellular nanowire-cell interfaces. The cell membrane and nanowire lipid coatings are marked with purple lines. (*d*) Electrical recordings from beating cardiomyocytes. (*i*) Extracellular recording. (*ii*) Transition from extracellular to intracellular recording during cellular entrance. (*iii*) Steady-state intracellular recording. The green and pink stars denote the peak positions of intracellular and extracellular signal components, respectively. Reprinted with permission from Reference 12. Copyright 2010, American Association for the Advancement of Science.

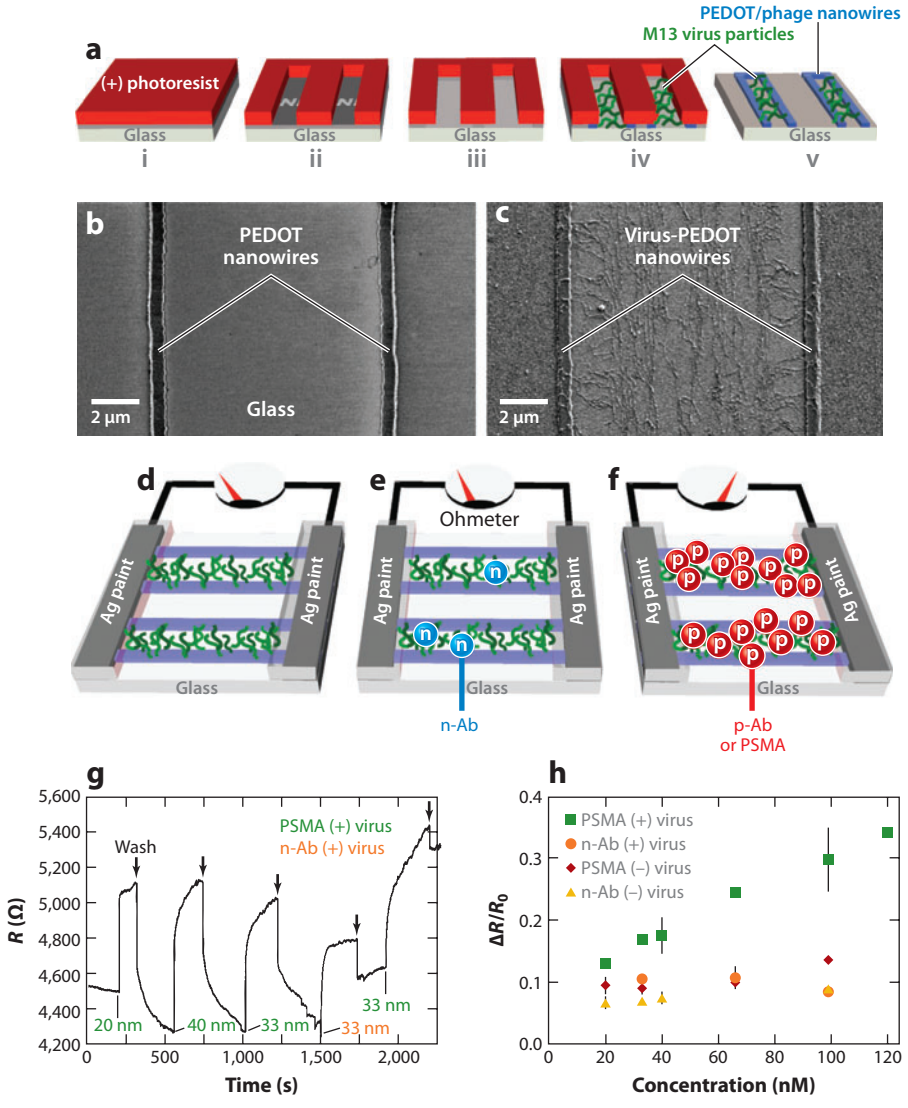

Figure 2

(*a*) Schematic diagram of the lithographically patterned nanowire electrodeposition process for the synthesis of virus-poly(3,4-ethylenedioxythiophene) (PEDOT) nanowires. (*b*) The resulting virus-nanowire device used for resistance-based measurements. (*c*) Schematic indicating little to no change in resistance after treatment with a nonbinding negative control antibody (n-Ab) (*blue circles*). (*d*) Depiction of the substantial change in resistance due to the presence of virus-binding positive antibody (p-Ab) (*red circles*). (*e*,*f*) Scanning electron micrographs of (*e*) pure PEDOT nanowires and (*f*) PEDOT nanowires with entrained M13 virus particles. (*g*) Real-time trace of raw biosensing data, showing injections of prostate-specific membrane antigen (PSMA) at the indicated concentrations (*green*) and an injection of a control, nonbinding antibody (*orange*). Black arrows indicate washes with PBF buffer. (*h*) A calibration curve compiled from real-time biosensing data. The change in resistance ($\Delta R/R_0$) following injection is plotted versus analyte concentration. A limit of detection of 20 nM was obtained for the detection of PSMA. Reprinted with permission from Reference 22. Copyright 2010, American Chemical Society.

M13 virus particles in addition to PEDOT, these filamentous particles became entrained into the PEDOT nanowires (**Figure 2*c***). We then configured these nanowires as chemiresistors and monitored wire resistance as a function of time as we exposed them to pulses of analyte molecules (**Figure 2*d–f***). Recently, we succeeded in detecting prostate-specific membrane antigen (PSMA), a prostate protein that is upregulated in cancerous tissue and expressed in urine. Arrays of ≈100 PEDOT-virus nanowires detected PSMA as a resistance increase of ≈2% to 5% (**Figure 2*f***). We established a limit of detection of 25 nM for PSMA in 140-mM buffer solutions (**Figure 2*g***). This study (26) also demonstrated the detection of PSMA in undiluted synthetic urine at 66 nM.

2.2. Nanowires Fabricated by Top-Down Processing

Top-down processing methods, in which semiconductor structures that are macroscale in at least one dimension are reduced to the nanometer scale to produce nanowires, have been explored in an attempt to increase the efficiency with which NWFETs are produced and, simultaneously, to increase the process's reproducibility and throughput. Williams et al. (30) performed the first top-down synthesis of silicon nanowires in 2004 by creating a protocol for fabricating silicon nanowires from commercially available SOI wafers. These SOI wafers consisted of a 50-nm silicon layer atop a 200-nm SiO_2 layer on silicon. These investigators obtained silicon nanowires with dimensions of 50 nm (height) × 60 nm (width) × 20 μm (length) by using electron-beam lithography (EBL), and they produced electrical contacts by using conventional optical lithography (30). They detected a single-stranded DNA (ssDNA) 12-mer at a concentration of 25 pM by using a complementary ssDNA probe, but no binding was detected for a single base–mismatched ssDNA sample at the same concentration (30). In 2005, Heath et al. (31) prepared arrays of silicon nanowires from SOI wafers by using a variant of the superlattice nanowire pattern transfer (SNAP) method (32). The DNA-sensing properties of these nanowires (33) are discussed further in Section 2.3, below.

In 2007, Reed et al. (34) highlighted the utility of top-down silicon nanowires for the detection of antibodies. In this study, Reed et al. used 50 nm × 25 nm silicon nanowires that were fabricated from SOI wafers and functionalized with anti-IgG and anti-IgA to detect 100 fM of IgG and IgA, respectively, with a high signal-to-noise ratio (>100). On the basis of this result, these authors predicted an ultimate limit of detection of 70 aM.

A persistent issue encountered in applications of nanowire-based biosensors to real physiological fluids, especially blood, is that the minute nanowire surface can be rapidly fouled by nonspecific protein adsorption. To eliminate this issue, Reed et al. (35) recently coupled SOI-derived silicon nanowire biosensors with a 5-μl microfluidic prechamber located upstream of the nanowires to preprocess blood. In this ingenious scheme, the capture antibodies for the biomarker of interest are located on the interior surface of a 5-μl microfluidic chamber and on the nanowire surface. The introduction of whole blood into this chamber permits the recognition and binding of the target molecule to these antibodies. Following a short equilibration period, the blood is transferred out of this chamber; the chamber is rinsed; and UV irradiation is used to release the bound target, which is flushed over the silicon nanowire sensors for detection and quantitation. An important advantage of this approach is the decoupling of the ionic strength of the blood from that of the rinsing buffer used for the detection of the target molecule by the nanowires. Use of this approach allowed two cancer markers, PMSA and CA15.3, to be detected in whole blood at concentrations of 1.5 ng ml^{-1} and 15 units ml^{-1}, respectively.

A clear advantage of the SOI top-down fabrication scheme is that one can prepare nanowires of virtually any width and thickness. In addition to control of the lateral dimension afforded by EBL and control of the height dimension by the parameters of the SOI wafer itself, nanowires can be reduced in size by corroding them in a controlled fashion. For example, in 2004 Juhasz et al.

(36) demonstrated that silicon nanowires prepared by EBL of SOI can be reduced in size down to minimum lateral dimensions of 9 nm and, simultaneously, smoothed by photoelectrochemical oxidation. In 2006, our group (37) demonstrated that kinetically controlled removal of material from nanowires by use of electrochemically induced corrosion reactions is a general way to reduce nanowire dimensions without inducing surface roughening.

This flexibility has enabled some of the first fundamental investigations of wire dimensions on biosensing performance. Elfstrom et al. (38) used single SOI silicon nanowires prepared with EBL to study the influence of wire diameter on the sensitivity of oxide-passivated silicon nanowires; the authors used pH detection as a model system. *p*-Type silicon nanowires were amine functionalized through the formation of a monolayer of 3-aminopropyltriethoxylsilane on the oxide surface. As in previous work (36), this group found that the conductivity of *p*-type silicon nanowires have *n*-type gate dependence, which is consistent with the presence of a conductivity-controlling inversion layer at the silicon/SiO_2 interface (38). As the wire width was reduced from 1 μm to ∼40 nm, an increase in the threshold voltage, V_{TH}, was observed from 1.4 V to 2.3 V, and simultaneously, the pH sensitivity of the nanowire increased dramatically. The calculations supporting this study (38) predict that nanowires at the lower end of this size continuum should have near–single charge sensitivity.

This analysis leaves open the possibility of achieving the minimum wire dimension required for high sensitivity along only one axis of the nanowire. In a 2008 study, Elfstrom et al. (39) explored the concept of reducing the thickness of SOI ribbons to 45 nm while retaining a micrometer-scale lateral dimension. The critical thickness required for this dimension is that of the Debye length, λ_D (39, 40):

$$\lambda_D = \sqrt{\frac{\varepsilon_0 \varepsilon_S k_B T}{q^2 N_B}}, \quad (2)$$

where ε_0 is the permittivity of free space, ε_S is the dielectric constant of the semiconductor, k_B is Boltzmann's constant, T is the temperature, q is the elementary charge, and N_B is the carrier concentration. For nanowire sensors whose thickness is equal to or less than λ_D, the charge of affinity-selected analyte molecules at the wire surface can electrostatically couple with electrons and holes within the nanowire, thereby altering the wire conductivity (39, 40). A value of 40 nm was obtained for λ_D through use of the parameters of the nanowires employed in this investigation. On the basis of this analysis, the authors assessed biotin-functionalized silicon nanowires with dimensions of 45 nm × 1 μm for the detection of streptavidin. They detected 6×10^{-13} M streptavidin, which corresponded to the binding of only 20 molecules at the nanowire surface (39). The main conclusion of this study is that excellent sensitivity can be achieved by shrinking just one wire dimension to values at or below λ_D.

A drawback of top-down nanowire fabrication schemes is that either EBL or fast ion bombardment (FIB)—both of which are time-consuming, expensive, and serial nanofabrication technologies—must be used to isolate a nanowire from the two-dimensional SOI layer. Carlen and coworkers (41, 42) have devised an elegant workaround for this problem (**Figure 3*a–d***). Their process is a simple elaboration of the baseline SOI process first used by Williams et al. (30): First, a silicon nitride etch mask is prepared on top of the [100]-oriented SOI wafer, and this mask is patterned by use of conventional lithography (**Figure 3*a***) (41, 42). Then, the SOI layer is wet etched to remove all the exposed silicon with an alkaline etchant, which selectively etches (101) plans of the silicon surface (**Figure 3*b***). The exposed [111] surfaces of the nascent nanowires are then thermally oxidized; the remaining SiN is removed (**Figure 3*c***); and the silicon mesa structure is reetched to isolate two silicon nanowires, both of which have a triangular cross section (**Figure 3*d***). This process uses only photolithography, no EBL or FIB is required, and minimum

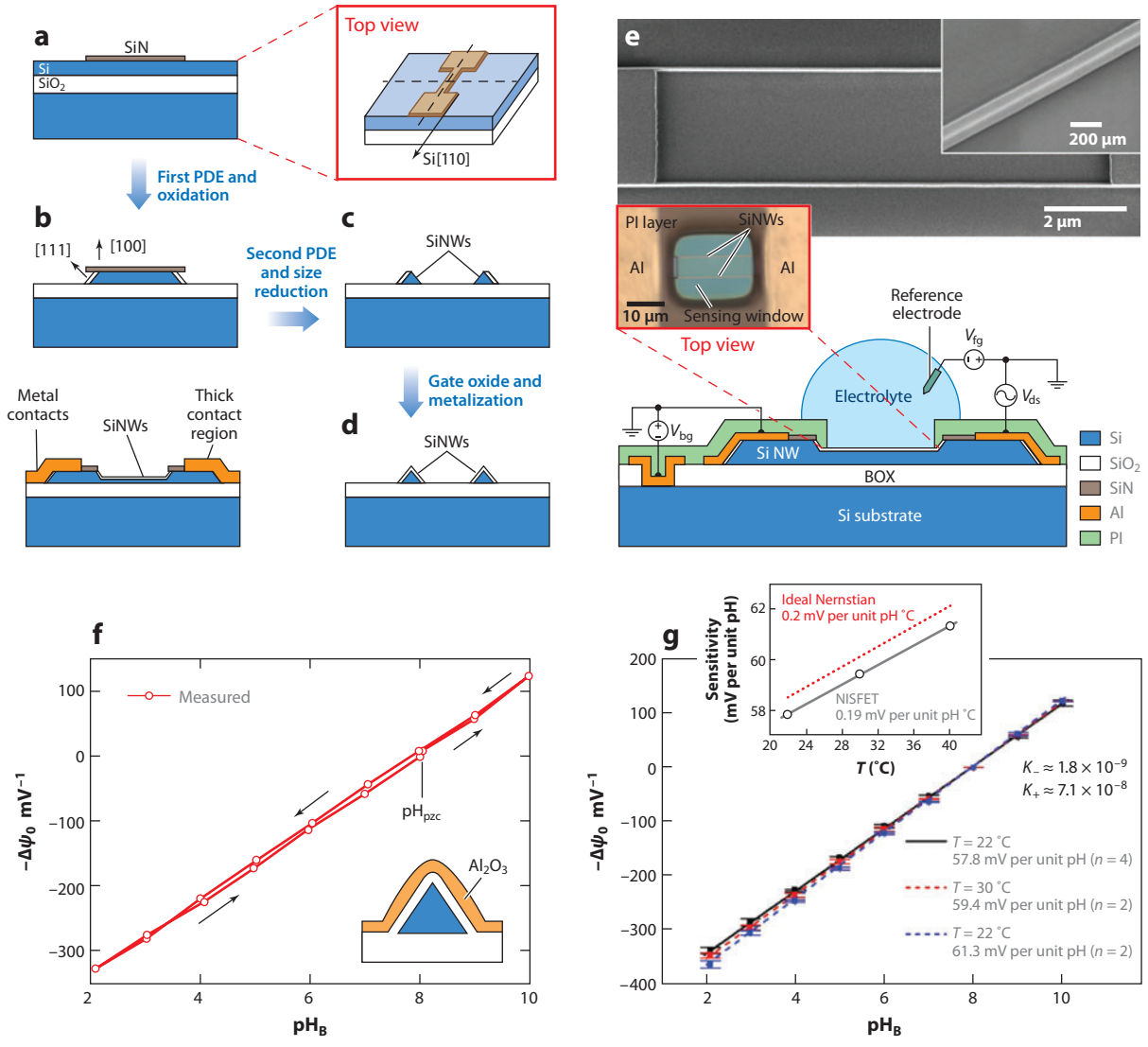

Figure 3

Top-down silicon nanowire (SiNW) microfabrication procedure (not to scale). (*a*) Initial lithography and etch steps for low-stress silicon nitride (SiN) layer patterning. (*b*) Silicon device layer plane-dependent wet etching (PDE) and local oxidation. (*c*) Second PDE and size reduction. (*d*) Gate oxidation and contact metallization. (*e*) High-resolution scanning electron microscopy images of fabricated SiNWs. Also shown is a schematic of electrical measurement. (*Inset*) Microscope image of a polyimide-encapsulated device prior to testing. (*f*,*g*) pH_B versus $\Delta\psi_0$ response of nanowires coated with Al_2O_3 through atomic layer deposition. (*f*) pH titration direction showing the response hysteresis. (*g*) The measured and fitted response for four different SiNW devices at a temperature of 22°C. Abbreviations: Al, aluminum; PI, polyimide. Panels *a* through *d* reprinted with permission from Reference 42. Copyright 2009, American Chemical Society. Panels *e* through *g* reprinted with permission from Reference 43. Copyright 2011, American Chemical Society.

nanowire dimensions down to 30 nm can be achieved (41, 42). One can configure the resulting nanowires as pH sensors (43) by covering them with a pH-responsive Al_2O_3 layer (thickness, 15 nm) using atomic layer deposition. Near-ideal Nerstian behavior for the oxide surface potential as a function of pH is then observed (57.8 mV per pH unit) (**Figure 3*f*,*g***).

2.3. Replacement of the Passivating Surface Oxide with a Molecular Monolayer

For silicon nanowires, the 1–2-nm-thick native oxide layer at the nanowire surface stabilizes the nanowire against oxidation in corrosive aqueous biological environments; however, like any gate oxide, it screens the silicon core of the nanowire from the charged analyte species captured by the bioaffinity layer on the oxide surface. Thus, there is a good reason to replace the native oxide layer with a thinner, covalent molecular monolayer that passivates the silicon surface.

In 2006, Heath et al. (33) described an example of this procedure. Beginning with arrays of top-down silicon nanowires prepared with the SNAP process (**Figure 4*a*,*b***) (32), the authors used UV light–assisted hydrosilation to attach a dense layer of t-BOC-protected C_{10} amine on freshly etched and hydrogen (H)-terminated silicon nanowires. Deprotection of the amine and reaction with the bifunctional linker GA enabled the attachment of uncharged peptide nucleic acid (PNAs) 16-mer strands, which completed the surface functionalization. The DNA-sensing properties of these oxide-free silicon nanowires were compared with those of silicon nanowires that had the normal native oxide and were functionalized with a monolayer of 3-aminopropyldimethylethoxysilane, which was subsequently conjugated with DNA through the same procedure employed with the oxide-free nanowires (33). Especially significant is that all these hybridization measurements were carried out at the full, 0.15-M ionic strength of the hybridization buffer saline–sodium citrate (1 × SSC). In terms of the sensing performance of these two types of nanowires, the oxide layer increased the relative resistance change, $\Delta R/R_0$, from <0.1 to ≈ 0.4 at 1 nM DNA (**Figure 4*c*,*d***). This increase in signal translated into a reduction in the limit of detection of two orders of magnitude, to 10 pM, at the oxide-free nanowires (**Figure 4*f***), which caused an expansion of the dynamic range for DNA detection by two orders of magnitude. The signal-to-noise ratio for DNA detection in this study was sufficient to enable the measurement of the kinetic rate constants for the binding and release of DNA molecules from the sensor surface. This study (33) was among the first to measure these critically important kinetic and thermodynamic binding metrics for nanowire-based sensors and to demonstrate sensing in high–ionic strength media.

In 2007, Gao et al. (44) demonstrated a different functionalization approach that involved the silanization of freshly etched nanowires with trimethyloxysilane aldehyde, which was subsequently reacted with amine-terminated PNA 21-mer capture probes. Arrays of an unspecified number of these nanowires, with radii ranging from 5 to 50 nm, demonstrated a limit of detection of 10 fM for the detection of fully complementary ssDNA 21-mers in a 40-mM tris buffer maintained at 50°C (44).

The following year, Zhang et al. (45) evaluated exactly the same passivation scheme as did Heath et al., but with three modifications:

1. As in the Gao et al. (44) study, uncharged PNA-capture strands were substituted for negatively charged DNA-capture strands, which removed the electrostatic repulsion that is normally present between ssDNA strands, thereby enhancing hybridization and in principle reducing the limits for DNA detection.
2. These PNAs were also longer 22-mers.
3. A 1:100 dilution of SSC was employed instead of full-strength SSC.

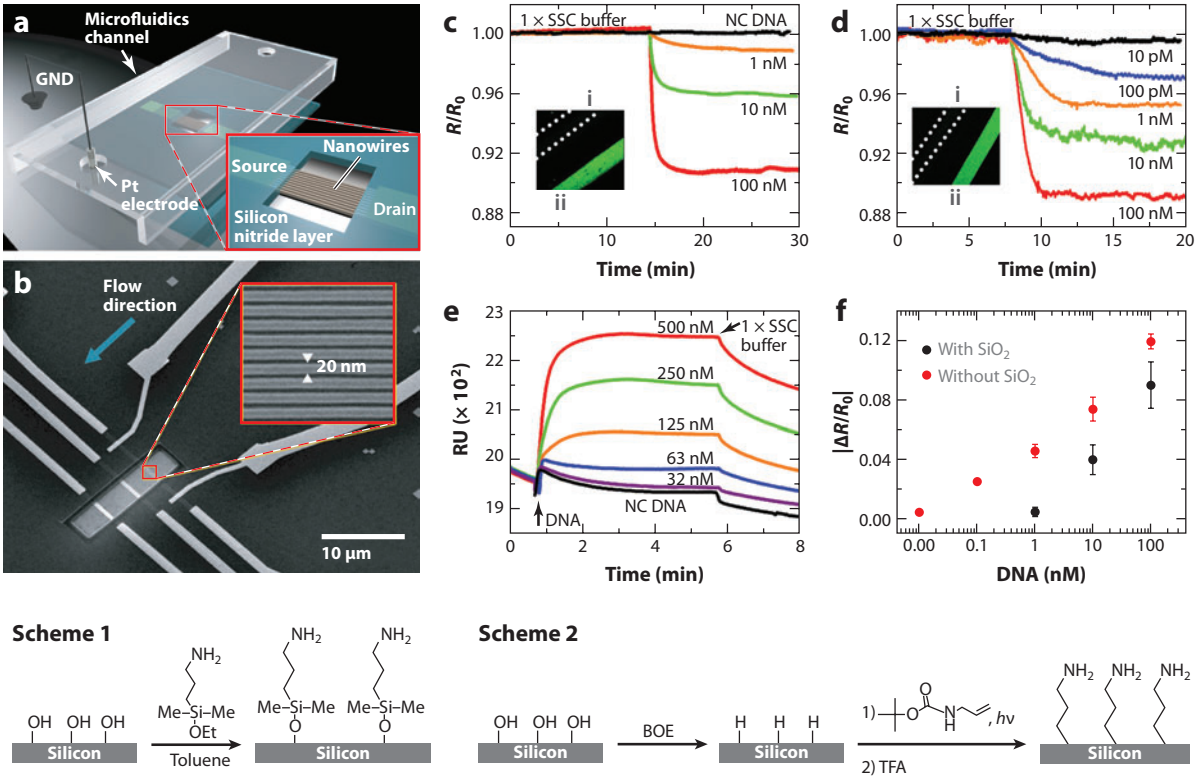

Figure 4

(*a*) Diagram of a single device section containing three groups of ≈10 silicon nanowires (SiNWs) prepared via the superlattice nanowire pattern transfer process in a microfluidic channel. The wafer is covered with Si_3N_4, except for an exposed active region covered with SiNWs. (*b*, *inset*) High-resolution scanning electron microscope image of 20-nm SiNWs. (*c–f*) Concentration-dependent, real-time sensing of complementary DNA by SiNWs and surface plasmon resonance (SPR) in a 0.165-M electrolyte. (*c*) Real-time responses of SiNWs that were surface functionalized according to Scheme 1 and coated with electrostatically adsorbed primary DNA. The black trace represents exposure of the SiNW sensors to 100 nM of noncomplementary (NC) single-stranded DNA. Each curve represents measurements from a different set of nanowires. (*Inset*) Fluorescence image of a Si(100) surface, with an overlaying polydimethylsiloxane (PDMS) microfluidics chip, followed by the addition of 10 nM of primary DNA, (*i*) 100 nM of NC fluorescent DNA, and (*ii*) 100 nM of complementary fluorescent DNA. The PDMS chip was removed before the image was collected. (*d*) Same as in panel *c*, except that the SiNWs were passivated with the monolayer. (*Inset*) Same as in the panel *c* inset, but the Si(100) surface was treated as in Scheme 2. (*e*) SPR measurement of the hybridization of complementary DNA to electrostatically adsorbed primary DNA on a poly-L-lysine surface. (*f*) Normalized SiNW responses for SiO_2-covered SiNWs (*black dots*) and bare SiNWs (*red dots*) as a function of the log of DNA concentration. For all measurements, the source-drain voltage was 50 mV. Abbreviations: BOE, buffered oxide etchant; GND, ground. Reprinted with permission from Reference 33. Copyright 2006, American Chemical Society.

Using transmission electron microscopy, Zhang et al. directly demonstrated that the SiO_2 layer on the nanowire was completely suppressed through this functionalization approach. Exposure to 1 nM of fully complementary DNA in a 0.01 × SSC hybridization buffer produced a resistance change, $\Delta R/R_0$, of 54%, whereas a 1-fM solution produced a $\Delta R/R_0$ of 6% (45). At a concentration of 1 nM, single base–mismatched ssDNA induced a resistance increase of 8%. A puzzling and unexplained aspect of this report is that these detection metrics were degraded when the 0.01 × SSC was replaced with deionized water (45).

3. CHEMICAL SENSORS

Most nanowire-based chemical sensing has involved the detection of gas-phase species via metal oxides, including ZnO, TiO_2, SnO_2, and others (4). Nanowires composed of conductive polymers, such as PT and Ppy, have also been widely used as chemical sensors for gases (46–48). Thin films of metal oxides, configured as resistors (so-called chemiresistors), have been employed extensively for this purpose (49–53) since Seiyama et al. (54) discovered metal oxide sensors in 1962. SnO_2 has been the canonical metal oxide for gas sensor applications since at least 1991, when Yamazoe and coworkers (55, 56) described key principles of the function of polycrystalline SnO_2 films. These authors studied the influence of grain diameter on sensor performance for the detection of H_2 and CO by *n*-type SnO_2 films for the first time. Reactions of these gases at the SnO_2 surface alter the surface's charge state, which, in turn, influences the accumulation or depletion of electrons within each grain. Upon exposure of SnO_2 films to either of these two reducing gases, the electrical resistance of the film is reduced, relative to that of pure air. Dramatic 6–15-fold increases in the amplitude of this resistance response were observed when the mean grain diameter, D_{ave}, was reduced across the range from 30 nm to 5 nm (56). The enhancement of sensitivity was attributed (56) to the reduction of D_{ave} to values smaller than the twice the Debye length, $2\lambda_D$. Single-crystal nanowires effectively constrict the conduction pathway to a single elongated grain; the wire diameter was functionally equivalent to D_{ave}. Thus, small nanowires allow the possibility of ultrasensitive analyte detection, provided that the same transduction mechanism operates.

Yang et al. (57) were among the first to demonstrate metal oxide nanowire–based chemical sensors: In 2002, they showed that bandgap-illuminated SnO_2 nanoribbons can detect NO_2 down to 3 ppm at room temperature. In that experiment, the authors postulated that NO_2 adsorption yields a surface NO_3 species that bridges two tin centers. The inductive withdrawal of electron density onto these NO_3 moieties from the *n*-type nanowire is responsible for the increase in nanowire resistance (58). At approximately the same time, Wang and coworkers (59) detected ethanol (250 ppm, 400°C), NO_2 (0.50 ppm, 200°C), and CO (250 ppm, 400°C) by using heated single-crystal SnO_2 nanobelts. Hundreds of papers describing the detection of molecules of In_2O_3 (60–62), TiO_2 (63–65), and ZnO (66–69), as well as other metal oxides, have appeared in the intervening nine years. At the frontier of this field are studies in which metal oxide nanowires were chemically modified to achieve selectivity for a particular analyte molecule or a family of molecules. These approaches have addressed a well-known shortcoming of SnO_2 and other metal oxides, namely cross-sensitivity to water vapor or, more generally, an absence of selectivity for a particular analyte molecule.

3.1. Functionalization of Metal Oxide Nanowires for Enhanced Selectivity

Strictly speaking, the introduction of a dopant species to a metal oxide nanowire should not be classified as functionalization, but dramatic changes in the function of SnO_2 nanowire–based ethanol sensors have been achieved (70) by *p*-doping such nanowires with antimony. In *n*-type SnO_2, exposure to ethanol reduces surface negative charge on the nanowire, reducing its resistance according to the following reactions (70):

$$SnO_2 \rightarrow Sn_{Sn} + 2O_o, \tag{3}$$

$$O_o \rightarrow V_o^{\cdot\cdot} + 1/2O_2 + 2e^-, \tag{4}$$

$$O + e^- \rightarrow O^-, \tag{5}$$

$$C_2H_5OH + 2O^- \rightarrow C_2H_5 + OH^- + O_2 + e^-. \tag{6}$$

This defect chemistry, in Kröger-Vink notation, is described in terms of O_o, an oxygen atom in an oxygen site, and $V_o^{\cdot\cdot}$, an oxygen atom vacancy with two negative charges. These reactions are identical for a *p*-type SnO_2 nanowire, but in such cases the reduction in the surface negative charge in Reaction 6 reduces, rather than increases, the resistance of the nanowire. Consistent with this expectation, *p*-type nanowires prepared by Wu (70) show an inverted response that is both rapid (seconds) and highly sensitive and that has an observed limit of detection of 40 ppm.

A straightforward, widely applied functionalization strategy is the immobilization of transition metal nanoparticles on the surfaces of metal oxide nanowires. Palladium (Pd) decoration of ZnO nanowires confers sensitivity to ethanol, as demonstrated by, for example, Lin et al. (71). Sensor-response amplitudes at ZnO nanowire mats were increased by a factor of two through the electrodeposition of Pd metal onto these nanowires from Pd^{2+} solution. Lin et al. reported a limit of detection of 5 ppm of ethanol (71).

Joshi et al. (66) showed that substitution of Au for Pd at ZnO nanowires increased the sensitivity to CO, particularly for nanowires operated at room temperature. At Au-decorated ZnO nanowire mats, CO was detectable at 100 ppm at room temperature with high signal to noise, but it was undetectable under identical conditions in the absence of Au, even for CO concentrations of up to 1,000 ppm (66). In the last two examples, which are typical of numerous studies in this category, the mechanism by which the metal imparted selectivity and alters sensor function was not apparent.

Among the most quantitative work in this direction is by Lee and coworkers (72), who studied the detection of ethanol at ZnO nanowire mats as a function of the loading of silver nanoparticles onto these nanowires (diameter ~50–100 nm). These authors examined the sensor's selectivity to ethanol versus NH_3, H_2, and CO for three discrete silver loadings of the nanowires (**Figure 5*a–d***). Significantly, an optimum silver loading—controlled by electron-beam evaporation—was observed in this study (**Figure 5*b***) in terms of both the sensor's sensitivity to ethanol and its selectivity for ethanol versus the other three gases. Raw sensor-response data (**Figure 5*e***) show that the addition of silver to the nanowire surface influences the amplitude of the sensor response but that the response and recovery times are unaffected. At the optimum silver loading, the ZnO nanowires were decorated with a high density of 3- to 8-nm-diameter silver nanoclusters, and ethanol at 100 ppm produced a signal of 228 (versus 5–8 for the other three gases) (72). ZnO nanowires with no silver produced signals of 67, whereas signals of 2 to 4 were observed for the other three gases. Higher loading of silver, consisting of larger-diameter silver nanoparticles, showed degraded signal amplitudes and degraded selectivities (**Figure 5*e*,*f***). Response and recovery times were weakly affected by silver modification of the ZnO nanowires; the optimized Ag-ZnO nanowires detected ethanol between 5 and 100 ppm in only 0.4 s and recovered from exposure over the same concentration range in 40 to 70 s (72).

The mechanism by which silver influences the sensor response is interesting (72): Nanowire resistance in the presence of ethanol is weakly affected at the lowest silver loading, and the increase in response amplitude arises almost entirely from an increase in the resistance of the nanowire in the absence of ethanol (**Figure 5*e***). Lee and colleagues postulate that in the absence of ethanol, silver contributes to the surface space charge of the nanowire, pinching off conduction and increasing the wire resistance. In the presence of ethanol, the surface's negative charge is extinguished, erasing the space charge at both silver-modified and silver-free SnO_2 nanowires (72). If this model is correct, metal modification involving high–work function metals should provide a general means by which the amplitude of sensor response to gases can be increased. More rigorous work will be required to understand the mechanism by which metals influence the sensing behavior of metal oxide nanowires.

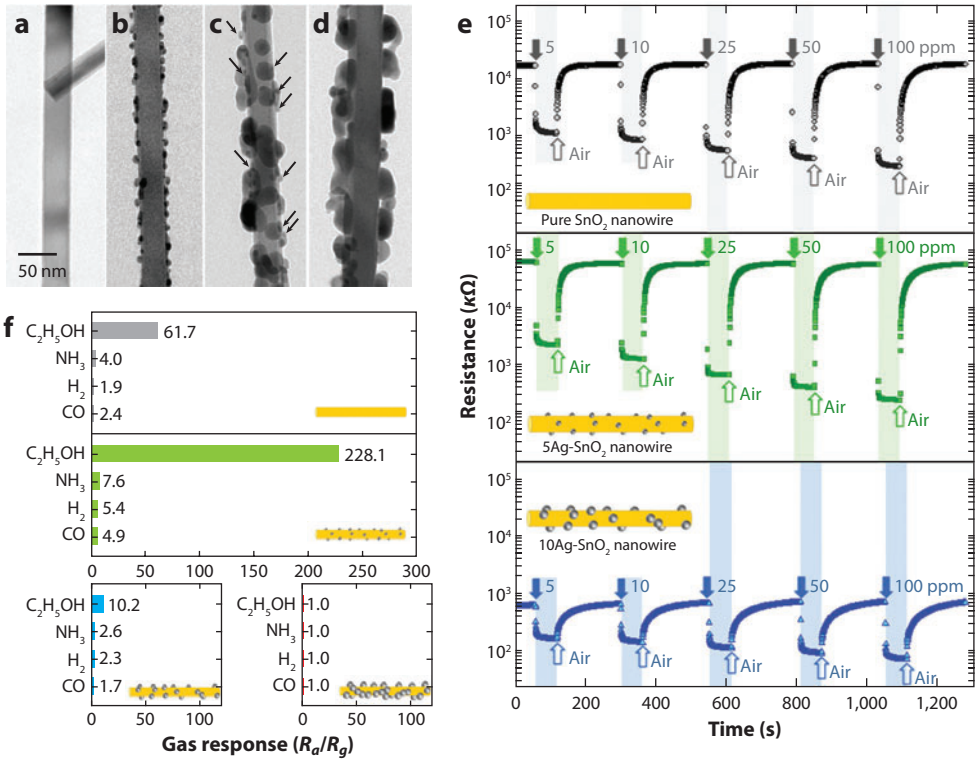

Figure 5

(*a–d*) Transmission electron micrographs of (*a*) a pure SnO_2 nanowire, (*b*) a 5Ag-SnO_2 nanowire, (*c*) a 10Ag-SnO_2 nanowire (*arrows indicate nanoparticles*), and (*d*) a 50Ag-SnO_2 nanowire following heat treatment at 450°C for 2 h. (*e*) C_2H_5OH-sensing transients for (*top*) a pure SnO_2 nanowire sensor, (*middle*) a 5Ag-SnO_2 nanowire sensor (that is, an array of SnO_2 nanowires onto which the equivalent of 5 nm of Ag was deposited through electron-beam evaporation), and (*bottom*) a 10Ag-SnO_2 nanowire sensor at 450°C. (*f*) Gas responses to 100 ppm of C_2H_5OH, NH_3, H_2, and CO at 450°C of sensors composed of the nanowires in panels *a* through *d*. The solid arrows indicate the time at which the ethanol vapor was introduced at the specified concentration. The open arrows indicate exposure to pure air. Reprinted with permission from Reference 72. Copyright 2011, American Chemical Society.

3.2. VO_2 Nanowire Sensors for Inert Gases Based on the Metal-to-Insulator Transition

The metal-to-insulator transition (MIT) of VO_2 is a first-order phase transition that occurs at 67°C; is characterized by an increase in electrical conductivity by two orders of magnitude or more (73); and in the case of VO_2 films, occurs on the timescale of nanoseconds (74). Kolmakov et al. (75) have demonstrated that the MIT of VO_2 nanowires provides a new mechanism for chemical sensing of the difficult-to-detect noble gases. Their basic idea is to use the MIT as a sensitive indicator of the thermal coupling between a suspended VO_2 nanowire and the surrounding ambient gases (**Figure 6*a***). The Joule heating induced by the application of a voltage ramp to the nanowire—from 5 V to 8 V in this case—produces a temperature ramp that spans the MIT temperature. The value of the voltage threshold for the MIT transition (V^+_{MIT} in **Figure 6*b***) is correlated with the thermal coupling of the nanowire to its gaseous ambient. For low pressures of the inert gas, little thermal transfer to the gas phase occurs, and the MIT is observed as a stepwise

increase of the current at a relatively low value of V^{+}_{MIT} as the voltage is increased. The V^{+}_{MIT} shifts to higher values as the capacity of the gas to cool the nanowire increases with its partial pressure (**Figure 6*c***). The sensitivity of the sensor is also inversely correlated with the molecular mass of the gas in a predictable way (**Figure 6*d***). The sensitivity of this novel sensing approach may permit the detection of helium at $P_{He} = 0.01$ Pa or $\approx 10^{-7}$ atm (75), but it is limited by the fact that the concentrations of components of a gas mixture cannot be individually resolved. The complete absence of selectivity in this case provides the opportunity to detect and measure the concentrations of noble gases.

Nanowires composed of β-$AgVO_3$ demonstrate bimodal resistance state-switching behavior that is similar to that reported for VO_2; in the former case, the switching is also triggered by voltage scanning (76). Single β-$AgVO_3$ nanowires have been used to detect H_2S, but in this case the MIT-like behavior did not serve as the basis for detection. Instead, H_2S was detected as a resistance decrease while the β-$AgVO_3$ nanowires were maintained in the conductive state. The authors of this study (76) reported a limit of detection for H_2S of 50 ppm; the response and recovery times were as low as 20 s.

3.3. Detection of Hydrogen by Palladium Nanowires

So far, metal nanowires have found few applications for chemical analysis. The detection of H by use of Pd nanowires, however, constitutes a special case because Pd can dissociatively adsorb H_2 and form a bulk hydride, PdH_x, where x saturates at ~0.7 (77). The formation of PdH_x can be detected as an increase in the electrical resistance of a Pd resistor ($\Delta R/R_0 \approx +90\%$ for $x = 0.7$) (77). In 2001, our group (1, 78) first attempted to detect H gas by using arrays of Pd nanowires. This initial work exposed an unforeseen problem with the use of Pd nanowires for H_2 sensing: The α phase–to–β phase transition of the PdH_x, and its attendant 3.3% lattice expansion (77), imposed a mechanical strain on the nanowire that induced fracturing, an effect that had not been observed in Pd film–based sensors (79, 80). Fractured nanowires showed no measurable electrical conductivity, but in the presence of H_2 above 1–2%, the threshold for the α phase–to–β phase transition, the so-called reswelling of the nanowires closed these fractures. This process rendered the nanowire electrically continuous, and a decrease in the electrical resistance of the nanowire or nanowires was observed (1, 78). This mechanism for detecting H_2 provides for the rapid detection of H_2 at high concentrations above 1–2%, and it has been exploited by H-sensing systems (81–85) that employ ensembles of Pd nanoparticles as resistors. However, because this mechanism is actuated by the α phase–to–β phase transition of the PdH_x, use of this mechanism to detect lower concentrations of H_2 is unreliable.

Recently, the problem of nanowire fracture in the H sensors demonstrated by Offermans et al. (86), Xiao et al. (87), and ourselves (88–90) has been solved. **Figure 7*a*** depicts a single Pd nanowire detector from our laboratory (89). Such fracture-resistant Pd nanowires (89, 90) enable the detection of H_2 from 0.0002% to 4% as an increase in the nanowire resistance, which reflects the higher electrical resistivity of PdH_x as x increases from 0 to 0.7 (**Figure 7*b–d***) (77). The lower limit of detection represents an extension of the dynamic range of these sensors by four orders of magnitude, compared with the earlier, fractured-wire devices. We are beginning to achieve a fundamental understanding of the chemical factors that influence sensor sensitivity and response and recovery rates. For example, at $[H_2]$ concentrations below 1%, the change in resistance, $\Delta R/R_0$, increases in direct proportion to $[H_2]^{1/2}$ (**Figure 7*e***), which is consistent with the equilibrium between gas-phase H_2 and chemisorbed H on the Pd surface: 0.5 H_2 (gas) → H (adsorbed) (89). Both the rate of sensor response and the rate of recovery are correlated with the surface area–to–volume ratio of the nanowire (**Figure 7*f***), which suggests that the rate-limiting

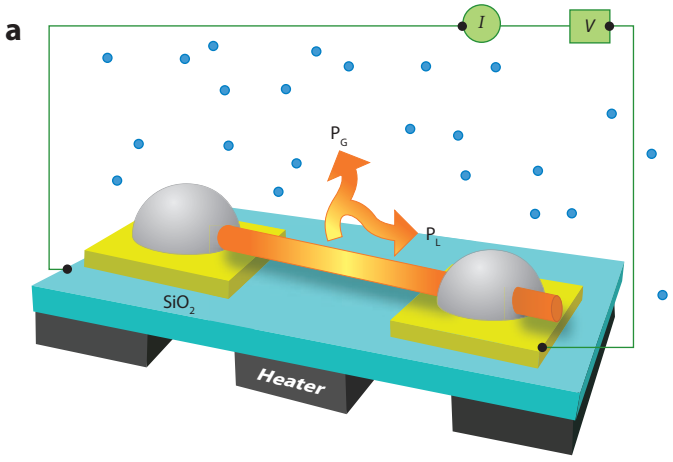

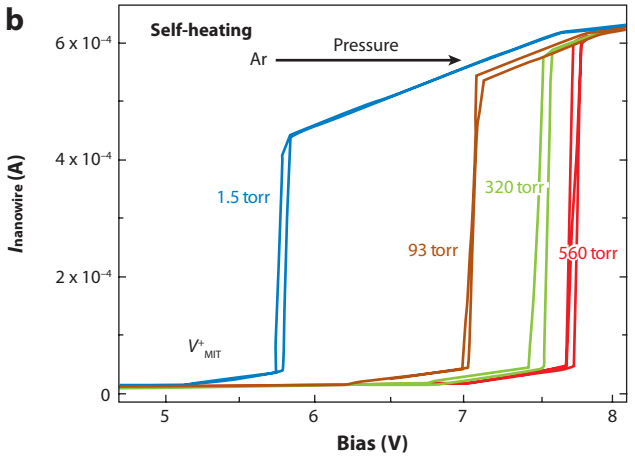

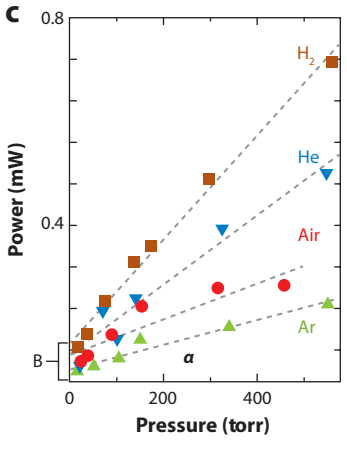

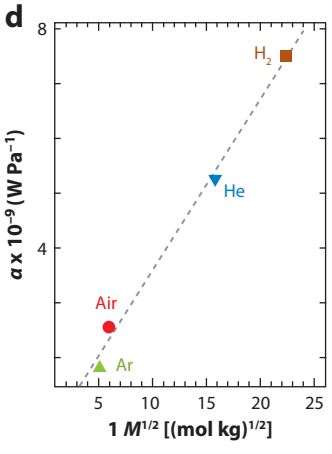

steps for both processes involve surface-limited chemical reactions. These reactions are believed to be the dissociative adsorption of H_2, in the case of sensor response, and the associative desorption of H from the Pd surface, in the case of sensor recovery (88, 89).

Compared with conventional Pd film resistance–based sensors (79), Pd nanowires operating at room temperature have response and recovery times that are an order of magnitude faster. However, response and recovery to H can be further accelerated by an additional factor of 50 through the use of nanowire Joule self-heating (88). The thermal activation of response and recovery derives (88) from rate-limiting dissociative H_2 adsorption (response) and associative H_2 desorption (recovery).

3.4. Polymeric Nanowires for Gas Sensing

Films of conductive polymers such as PANI, PPy, PT, and PEDOT have been employed in chemical sensors (46–48). The implementation of these materials in nanowire-based sensors has recently been reviewed (91, 92).

Since 2003, research into conducting polymer–based chemical sensors has been propelled by three innovations involving the synthesis of these nanowires. First, Weiller et al. (93) demonstrated that bulk quantities of PANI nanowires can be prepared via an interfacial polymerization technique at the chloroform-water interface. The resulting three-dimensional nanowire networks are highly branched, and the authors demonstrated control of nanofibers ranging in diameter from 30 nm to 120 nm on the basis of the type of acid present in the aqueous phase (94, 95). Second, Doshi & Reneker (96) and Reneker & Chun (97) used the electrospinning method to fabricate ultralong (>100-μm) unbranched nanowires of conductive polymers. The accessibility of electrospun nanofibers for chemical sensing applications was improved in 2003, when Xia et al. (98) and Xia & Li (99) elaborated on the basic electrospinning apparatus by adding a gap to the receiver surface, across which a second electric field could be applied. Electrospun polymer nanowires oriented along this field, between these two electrodes and these receiver electrodes, were subsequently used to probe the electrical properties of the nanofibers or to carry out chemiresistive chemical sensing investigations. Third, Myung and colleagues (16) and Yun et al. (15) simultaneously demonstrated that electrodeposition can be exploited to synthesize a single conductive polymer nanowire in a prefabricated gap between two shaped metal electrodes. As with the electrospinning operation developed by Xia et al., this process enabled the preparation of a conductive polymer nanowire–based chemiresistor in a single electrochemical synthesis operation.

On the heels of these synthesis innovations came a flurry of chemical sensing studies on conductive polymer nanowires wherein the nanowires were configured as chemiresistors. Weiller et al. (93) used mats of PANI nanofibers to detect 100 ppm of NH_3 by the acid state of the polymer as a resistance increase of seven orders of magnitude and 100 ppm of HCl by the basic state

Figure 6

(*a*) The design and principle of operation of a VO_2 nanowire metal-to-insulator transition (MIT) gas sensor. P_G and P_L indicate heat fluxes dissipating into the gas environment and metal contacts, respectively. (*b*) Current-voltage (*I-V*) scans of a self-heated nanowire at different argon (Ar) pressures show typical onset of MIT (forward direction) as well as the typical scatter in transition voltage. The cooling (metal-to-insulator) part of the curve is hysteretic; V_{MIT} is beyond the bias voltage region shown in the figure. (*c*) Transition power–versus–gas pressure graph for the self-heated nanowire and four different gases (the slope of this graph defines the *R* parameter). (*d*) The experimental data for the *R* parameter, showing its linear dependence on the reciprocal square root of the molar mass of the gases. Reprinted with permission from Reference 75. Copyright 2009, American Chemical Society.

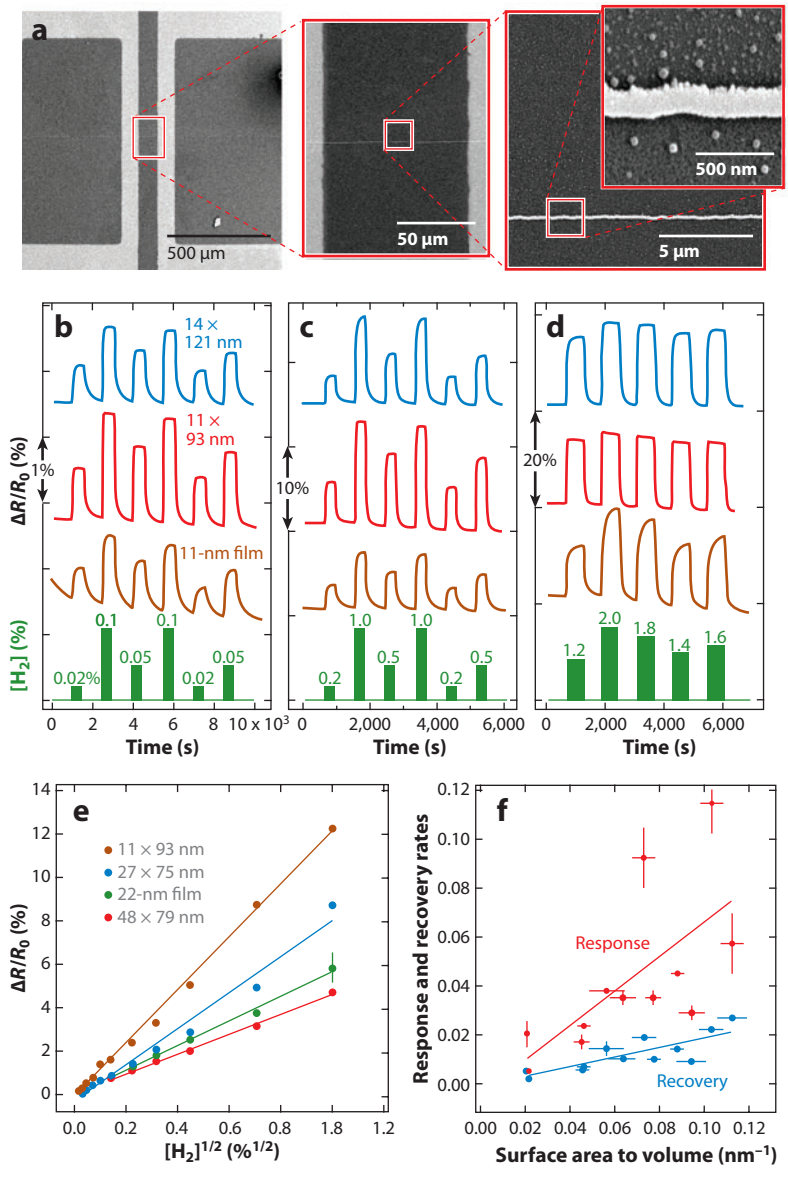

Figure 7

(*a*) A palladium (Pd) nanowire sensor consisting of a single, linear Pd nanowire of defined thickness and width with two evaporated gold contacts at either 50 or 100 µm. (*b–d*) Hydrogen (H)-sensing data for three devices with similar Pd thicknesses: a 14 nm × 121 nm nanowire, an 11 nm × 93 nm nanowire, and an 11 nm × 100 µm film. The H concentration program is plotted in green at the bottom of each data set. (*e*) For $[H_2]$ ranging from very low concentrations to 1%, $\Delta R/R_0$ is approximately proportional to $[H_2]$. (*f*) Plot of the sensor response rate (*red*) and the recovery rate (*blue*) as a function of the surface area–to–volume ratio. Reprinted with permission from Reference 89. Copyright 2010, American Chemical Society.

of the polymer as a resistance decrease of two orders of magnitude. Both the amplitude of the observed resistance changes and the response/recovery times were enhanced for PANI nanofibers as compared with PANI films. An investigation of the response of PANI nanofibers to hydrazine, chloroform, and methanol showed that several mechanisms operate in parallel to produce the observe resistance changes in these materials (100). In 2004, Craighead et al. (101) showed that single nanowires of PANI prepared through electrospinning can function as ammonia sensors. In the presence of ammonia, the electrical resistance of a single 355-nm-diameter PANI nanowire increased by up to ~10-fold. The mechanism of this response is probably the reaction between NH_3 and the protonated imine nitrogens of the PANI. NH_3 concentrations down to 0.5 ppm were detectable, but response and recovery times, limited by the diffusion of NH_3 in the polymer, ranged from 200 to 400 s. Time-independent sensor responses were not observed for these systems, except at a relatively high [NH_3] of 50 ppm (101).

The capabilities of conductive polymer nanowire sensors for gas sensing have advanced considerably since these early experiments. Myung et al. (102) recently employed the LPNE synthesis method (23–25) to fabricate single PPy nanoribbons with lateral dimensions of 25 nm (height) and 300 to 500 nm (width) (**Figure 8*a***). Through this process, a single PPy nanowire (**Figure 8*d***) can be patterned onto dielectrics such as oxidized silicon wafers (**Figure 8*c***) and flexible polyimide films (**Figure 8*b***). Myung et al. subsequently assessed the properties of PPy nanoribbons for detecting ammonia vapor in a chemiresistor configuration. The electrical resistance of these nanoribbons, R_0, was adjusted from ~6.5 S cm^{-1} to 0.003 S cm^{-1} by exposure to NaOH following electrodeposition. Exposure of these nanoribbons to ammonia vapor induced an additional increase in the resistance: $\Delta R/R_0$ increased by nearly 10-fold over this range of R_0 (**Figure 8*e***), an effect that is attributed to an increase in λ_D in the polymer with decreasing dopant density (102). These PPy nanoribbons showed relatively rapid resistance changes of 3 to 7 min—an order of magnitude faster than observed for single 355-nm-diameter PANI nanowires in previous work (101)—and the authors reported a limit of detection of 0.6 ppm for the 0.003 S cm^{-1} devices (**Figure 8*f***) (102).

As in the case of polymer nanowire–based biosensors, the nature of the electrical contacts to a polymer nanowire can determine how, or even whether, a particular analyte molecule is detected. For example, Weiller et al. (103) demonstrated that PANI nanowire networks show that $\Delta R/R_0 = -3\%$ upon exposure to [H_2] = 1% for PANI nanowires with Au contacts; however, $\Delta R/R_0 = +65\%$ is observed for the same experiment when platinum (Pt) contacts are employed. The temporal properties of the detection are also affected; the Pt contacts yield significantly slower response and recovery times. The influence of the contacting metal is attributed (103) to both the spontaneous formation of Pt hydride at the Pt-PANI interface and the fact that Au has no stable hydride phase. More specifically, for PANI nanowires with Au contacts, investigators have proposed (104) that H_2 forms H bonds to the amine nitrogens along the PANI backbone and then dissociates, mimicking the influence of strong acids on the PANI conductivity. However the Pt-PANI interfacial resistance increases upon exposure to H_2, presumably because the formation of a Pt-H monolayer at this interface imposes a barrier to charge transfer. Such a barrier may arise from the lowering of the Pt work function by H adsorption, which would cause the formation of a Schottky barrier with the *p*-type PANI nanowire (103). Importantly, this research shows that the influence of electrical contacts can be prevalent in sensing measurements that involve organic polymers.

Although the vast majority of nanowire-based chemical sensors involve resistance-based transduction, Tong and coworkers (105) recently described the use of single nanofibers composed of either a PANI/polystyrene (PANI/PS) composite or bromothymol blue (BTB)-doped poly(methylmethacrylate) (PMMA) for the detection of NO_2 and NH_3, respectively. In this case,

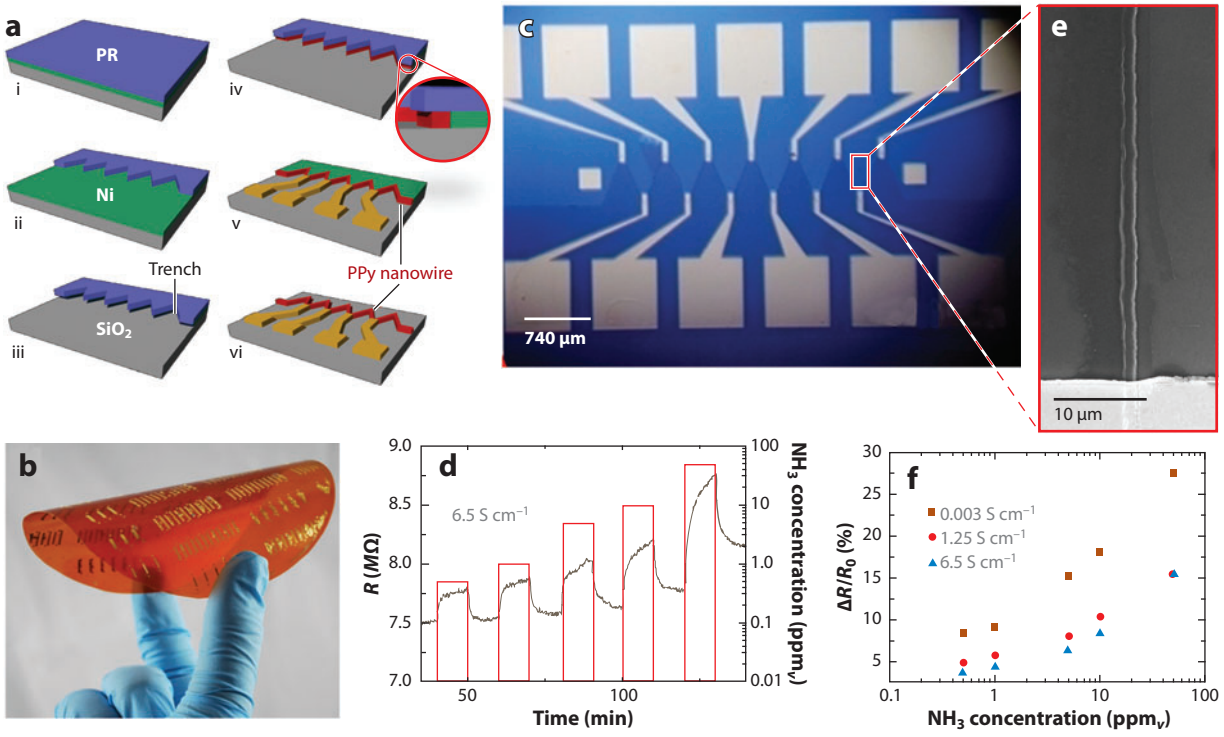

Figure 8

(*a*) Schematic illustration of the modified lithographically patterned nanowire electrodeposition (LPNE) process. (*i*) A sacrificial layer of nickel (Ni; green) is deposited by electron beam onto substrates, followed by spin coating of photoresist (PR). (*ii*) The PR is photopatterned by exposing the spin-coated sample to UV light. The exposed PR is then dissolved by developer solution. (*iii*) The exposed Ni is removed by chemical etching; thereafter, electrochemical etching is used to produce Ni nanobands. (*iv*) Polypyrrole (PPy) nanoribbons are electropolymerized at the Ni nanobands. (*v*) The PR is removed, and gold electrodes are photopatterned. (*vi*) The Ni is removed. (*b*) Flexible polyimide films can be used as substrates for this LPNE PPy nanoribbon–fabrication process, (*c*) An example of a complete PPy nanoribbon sensor fabricated on oxidized silicon. (*d*) Response of a 6.5 S cm^{-1} PPy nanoribbon to ammonia vapor. The brown line shows the sensor's response, and the red line shows the concentration and duration of the NH_3 exposures. (*e*) Scanning electrode microscope image of a single PPy nanowire integrated with gold electrodes. (*f*) Calibration plot showing the response amplitude as a function of [NH_3] for three PPy nanoribbon sensors with conductivities of 0.003 S cm^{-1} (*brown*), 1.25 S cm^{-1} (*red*), and 6.5 S cm^{-1} (*blue*). Reprinted with permission from Reference 102. Copyright 2010, American Chemical Society.

however, exposure to these two gases is detected as a change in the optical absorbance of these nanofibers (diameter ≈ 250 nm) when they are configured as transmission waveguides. Upon exposure to NO_2, for example, PANI/PS nanowires showed a rapid (millisecond-range) increase in absorbance at $\lambda = 532$ nm that was readily detectable (≈0.1 absorbance units) for [NO_2] = 0.1 ppm (105). Recovery of the PANI/PS nanofibers required a much longer period of up to 1,500 s, and the pronounced asymmetry of the response and recovery times is not understood. The authors observed a very similar response at $\lambda = 660$ nm upon the exposure of BTB-PMMA nanofibers to NH_3; again, there was a rapid response, a retarded recovery, and an appreciable response (0.1 absorbance units) at [NH_3] = 3 ppm. The ultrafast response of these devices—as fast as 30 ms in some experiments (105)—has not been reported for any other nanowire-based sensing schemes, and it certainly justifies more intensive investigation of the mechanism of sensor response.

4. SUMMARY

In this review, we highlight only a minute fraction of the amazing results reported in the literature. Some conclusions pertaining to the overall field of nanowire-based sensing are nevertheless apparent, even from this incomplete sampling. The most important conclusion is that nanowire-based chemical and biosensor technology is approaching viability for several applications. Metrics relating to sensor sensitivity and speed have been achieved for various analyte systems. However, to our knowledge, nanowire sensors are not yet commercially available for any application. What do we still need to understand about the function of nanowire-based sensors and biosensors to improve them further?

The dazzling performance achieved by these devices was obtained mainly through the empirical optimization of individual systems. Still missing is a complete, fundamental understanding of the mechanisms of sensor function, both for biosensors and for chemical sensors. Also, progress toward a fundamental understanding of sensor function is profoundly uneven across the sensor landscape: Silicon nanowires in biosensors are probably the best-understood nanowire sensing technology. The diversity of metal oxide nanowire–based gas sensors are less well understood in general, in part because many materials have been employed and many analyte species studied. Even more rudimentary is our understanding of signal transduction in polymer nanowires in any of the sensing applications in which they have been exploited so far, with the possible exception of pH sensors. Investigations of the influence of nanowire dimensions on sensing metrics are only beginning to be reported (e.g., Reference 39), and much more work in this direction is needed. The influence of the electrical contacts on the sensing behavior and the nature of the supporting surface for the nanowire(s) are two important issues that have hardly been investigated. As indicated above, the transduction mechanisms that operate in polymer-based sensors and biosensors are particularly mysterious, but the remarkable sensing performance highlighted in this review, for both chemical sensors and biosensors, justifies further systematic work to elucidate these mechanisms.

Competition between bottom-up and top-down nanowires has emerged, but neither approach is clearly ascendant. In the specific case of silicon, top-down nanowires fashioned from SOI wafers provide for simplified processing, but whether transport metrics in these nanowires are better than those in state-of-the-art VLS silicon nanowires is unknown. This field would benefit from direct comparisons between VLS and SOI silicon nanowires by disinterested individual research groups.

Chemical sensing has focused on sensitivity, limits of detection, and optimization of the response and recovery time, and tremendous progress has been made for several systems. Selectivity has often been neglected, and this area would benefit from more research that addresses this critically important issue.

DISCLOSURE STATEMENT

The author is not aware of any affiliations, memberships, funding, or financial holdings that might be perceived as affecting the objectivity of this review.

ACKNOWLEDGMENTS

My research in the area of nanowire-based chemical sensing and biosensing is supported by the National Science Foundation through contract CHE-0956524.

LITERATURE CITED

1. Penner RM, Favier F, Walter EC, Zach MP, Benter T. 2001. Hydrogen sensors and switches from electrodeposited palladium mesowire arrays. *Science* 293:2227–31
2. Lieber CM, Cui Y, Wei QQ, Park HK. 2001. Nanowire nanosensors for highly sensitive and selective detection of biological and chemical species. *Science* 293:1289–92
3. Zacharias M, Ramgir NS, Yang Y. 2010. Nanowire-based sensors. *Small* 6:1705–22
4. Kolmakov A, Moskovits M. 2004. Chemical sensing and catalysis by one-dimensional metal-oxide nanostructures. *Annu. Rev. Mater. Res.* 34:151–80
5. Kwon YK, Lee M, Baik KY, Noah M, Lee JO, Hong S. 2009. Nanowire and nanotube transistors for lab-on-a-chip applications. *Lab Chip* 9:2267–80
6. Lieber CM, Patolsky F, Zheng GF. 2006. Nanowire-based biosensors. *Anal. Chem.* 78:4260–69
7. Bergveld P. 1972. Development, operation, and application of the ion-sensitive field-effect transistor as a tool for electrophysiology. *IEEE Trans. Biomed. Eng.* 19:342–51
8. Bergveld P. 1970. Development of an ion-sensitive solid-state device for neurophysiological measurements. *IEEE Trans. Biomed. Eng.* 17:70–71
9. Israelachvili JN. 2011. *Intermolecular and Surface Forces*. Burlington, MA: Academic. 674 pp.
10. Manalis SR, Fritz J, Cooper EB, Gaudet S, Sorger PK. 2002. Electronic detection of DNA by its intrinsic molecular charge. *Proc. Natl. Acad. Sci. USA* 99:14142–46
11. Lieber CM, Tian BZ, Cohen-Karni T, Qing Q, Duan XJ, Xie P. 2010. Three-dimensional, flexible nanoscale field-effect transistors as localized bioprobes. *Science* 329:830–34
12. Tian B, Cohen-Karni T, Qing Q, Duan X, Xie P, et al. 2010. Three-dimensional, flexible nanoscale field-effect transistors as localized bioprobes. *Science* 329:831–34
13. Lieber CM, Cohen-Karni T, Timko BP, Weiss LE. 2009. Flexible electrical recording from cells using nanowire transistor arrays. *Proc. Natl. Acad. Sci. USA* 106:7309–13
14. Ramanathan K, Bangar MA, Yun M, Chen W, Myung NV, Mulchandani A. 2005. Bioaffinity sensing using biologically functionalized conducting-polymer nanowire. *J. Am. Chem. Soc.* 127:496–97
15. Yun MH, Myung NV, Vasquez RP, Lee CS, Menke E, Penner RM. 2004. Electrochemically grown wires for individually addressable sensor arrays. *Nano Lett.* 4:419–22
16. Mulchandani A, Ramanathan K, Bangar MA, Yun MH, Chen WF, Myung NV. 2004. Individually addressable conducting polymer nanowires array. *Nano Lett.* 4:1237–39
17. Mulchandani A, Shirale DJ, Bangar MA, Chen W, Myung NV. 2010. Effect of aspect ratio (length:diameter) on a single polypyrrole nanowire FET device. *J. Phys. Chem. C* 114:13375–80
18. Mulchandani A, Bangar MA, Shirale DJ, Chen W, Myung NV. 2009. Single conducting polymer nanowire chemiresistive label-free immunosensor for cancer biomarker. *Anal. Chem.* 81:2168–75
19. Yun MH, Luo XL, Lee I, Huang JY, Cui XYT. 2011. Ultrasensitive protein detection using an aptamer-functionalized single polyaniline nanowire. *Chem. Commun.* 47:6368–70
20. Yun M, Lee I, Luo XL, Cui XT. 2011. Highly sensitive single polyaniline nanowire biosensor for the detection of immunoglobulin G and myoglobin. *Biosens. Bioelectron.* 26:3297–302
21. Penner RM, Donavan KC, Arter JA, Pilolli R, Cioffi N, Weiss GA. 2011. Virus-poly(3,4-ethylenedioxythiophene) composite films for impedance-based biosensing. *Anal. Chem.* 83:2420–24
22. Penner RM, Arter JA, Taggart DK, McIntire TM, Weiss GA. 2010. Virus-PEDOT nanowires for biosensing. *Nano Lett.* 10:4858–62
23. Penner RM, Xiang CX, Yang YG. 2009. Cheating the diffraction limit: electrodeposited nanowires patterned by photolithography. *Chem. Commun.* 2009:859–73
24. Penner RM, Xiang CX, Kung SC, Taggart DK, Yang F, et al. 2008. Lithographically patterned nanowire electrodeposition: a method for patterning electrically continuous metal nanowires on dielectrics. *Am. Chem. Soc. Nano* 2:1939–49
25. Penner RM, Menke EJ, Thompson MA, Xiang C, Yang LC. 2006. Lithographically patterned nanowire electrodeposition. *Nat. Mater.* 5:914–19
26. Weiss GA, Penner RM. 2008. The promise of phage display: customized affinity and specificity. *Anal. Chem.* 80:3082–89

27. Weiss GA, Yang LMC, Diaz JE, McIntire TM, Penner RM. 2008. Covalent virus layer for mass-based biosensing. *Anal. Chem.* 80:933–43
28. Weiss GA, Yang LMC, Diaz JE, McIntire TM, Penner RM. 2008. Direct electrical transduction of antibody binding to a covalent virus layer using electrochemical impedance. *Anal. Chem.* 80:5695–705
29. Weiss GA, Yang LMC, Tam PY, Murray BJ, McIntire TM, et al. 2006. Virus electrodes for universal biodetection. *Anal. Chem.* 78:3265–70
30. Williams RS, Jung GY, Johnston-Halperin E, Wu W, Yu ZN, et al. 2006. Circuit fabrication at 17 nm half-pitch by nanoimprint lithography. *Nano Lett.* 6:351–54
31. Heath JR, Beckman R, Johnston-Halperin E, Luo Y, Green JE. 2005. Bridging dimensions: demultiplexing ultrahigh-density nanowire circuits. *Science* 310:465–68
32. Heath JR, Melosh NA, Boukai A, Diana F, Gerardot B, et al. 2003. Ultrahigh-density nanowire lattices and circuits. *Science* 300:112–15
33. Heath JR, Bunimovich YL, Shin YS, Yeo WS, Amori M, Kwong G. 2006. Quantitative real-time measurements of DNA hybridization with alkylated nonoxidized silicon nanowires in electrolyte solution. *J. Am. Chem. Soc.* 128:16323–31
34. Reed MA, Stern E, Klemic JF, Routenberg DA, Wyrembak PN, et al. 2007. Label-free immunodetection with CMOS-compatible semiconducting nanowires. *Nature* 445:519–22
35. Reed MA, Stern E, Vacic A, Rajan NK, Criscione JM, et al. 2010. Label-free biomarker detection from whole blood. *Nat. Nanotechnol.* 5:138–42
36. Juhasz R, Elfstrom N, Linnros J. 2005. Controlled fabrication of silicon nanowires by electron beam lithography and electrochemical size reduction. *Nano Lett.* 5:275–80
37. Penner RM, Thompson MA, Menke EJ, Martens CC. 2006. Shrinking nanowires by kinetically controlled electrooxidation. *J. Phys. Chem. B* 110:36–41
38. Elfstrom N, Juhasz R, Sychugov I, Engfeldt T, Karlstrom AE, Linnros J. 2007. Surface charge sensitivity of silicon nanowires: size dependence. *Nano Lett.* 7:2608–12
39. Elfstrom N, Karlstrom AE, Linnrost J. 2008. Silicon nanoribbons for electrical detection of biomolecules. *Nano Lett.* 8:945–49
40. Fahmy TM, Stern E, Wagner R, Sigworth FJ, Breaker R, Reed MA. 2007. Importance of the Debye screening length on nanowire field effect transistor sensors. *Nano Lett.* 7:3405–9
41. Tong HD, Chen S, van der Wiel WG, Carlen ET, van den Berg A. 2009. Novel top-down wafer-scale fabrication of single crystal silicon nanowires. *Nano Lett.* 9:1015–22
42. Carlen ET, Chen SY, Bomer JG, van der Wiel WG, van den Berg A. 2009. Top-down fabrication of sub-30-nm monocrystalline silicon nanowires using conventional microfabrication. *Am. Chem. Soc. Nano* 3:3485–92
43. Carlen ET, Chen SY, Bomer JG, van den Berg A. 2011. Al_2O_3/silicon nanoISFET with near ideal Nernstian response. *Nano Lett.* 11:2334–41
44. Gao ZQ, Agarwal A, Trigg AD, Singh N, Fang C, et al. 2007. Silicon nanowire arrays for label-free detection of DNA. *Anal. Chem.* 79:3291–97
45. Zhang GJ, Chua JH, Chee RE, Agarwal A, Wong SM, et al. 2008. Highly sensitive measurements of PNA-DNA hybridization using oxide-etched silicon nanowire biosensors. *Biosens. Bioelectron.* 23:1701–7
46. Janata J, Josowicz M. 2003. Conducting polymers in electronic chemical sensors. *Nat. Mater.* 2:19–24
47. Sadik OA. 1999. Bioaffinity sensors based on conducting polymers: a short review. *Electroanalysis* 11:839–44
48. Wallace GG, Nguyen TA, Barisci JN, Partridge A. 2003. Investigation of conducting polymer materials for sensor array. *Synth. Metals* 137:1445–46
49. Pallás-Areny R, Webster JG. 2001. *Sensors and Signal Conditioning*. New York: Wiley. 587 pp.
50. Gopel W. 1996. Nanosensors and molecular recognition. *Microelectron. Eng.* 32:75–110
51. Gopel W. 1996. Ultimate limits in the miniaturization of chemical sensors. *Sens. Actuators Phys.* 56:83–102
52. Sberveglieri G. 1992. *Gas Sensors: Principles, Operation, and Developments*. Dordrecht, Neth./Boston: Kulwer Acad. 409 pp.
53. Comini E, Faglia G, Sberveglieri G. 2009. *Solid State Gas Sensing*. New York: Springer. 337 pp.

54. Seiyama T, Kato A, Fujiishi K, Nagatani M. 1962. A new detector for gaseous components using semiconductive thin films. *Anal. Chem.* 34:1502–3
55. Yamazoe N. 1991. New approaches for improving semiconductor gas sensors. *Sens. Actuators B Chem.* 5:7–19
56. Xu CN, Tamaki J, Miura N, Yamazoe N. 1991. Grain-size effects on gas sensitivity of porous SnO_2-based elements. *Sens. Actuators B Chem.* 3:147–55
57. Yang PD, Law M, Kind H, Messer B, Kim F. 2002. Photochemical sensing of NO_2 with SnO_2 nanoribbon nanosensors at room temperature. *Angew. Chem. Int. Ed.* 41:2405–8
58. Maiti A, Rodriguez JA, Law M, Kung P, McKinney JR, Yang PD. 2003. SnO_2 nanoribbons as NO_2 sensors: insights from first principles calculations. *Nano Lett.* 3:1025–28
59. Comini E, Faglia G, Sberveglieri G, Pan ZW, Wang ZL. 2002. Stable and highly sensitive gas sensors based on semiconducting oxide nanobelts. *Appl. Phys. Lett.* 81:1869–71
60. Mehta BR, Kumar M, Singh VN, Chatterjee R, Milikisiyants S, et al. 2010. The role of stoichiometry of indium and oxygen on gas sensing properties of indium oxide nanostructures. *Appl. Phys. Lett.* 96:123114
61. Zhou WL, Zeng ZM, Wang K, Zhang ZX, Chen JJ. 2009. The detection of H_2S at room temperature by using individual indium oxide nanowire transistors. *Nanotechnology* 20:045503
62. Lu JG, Fan ZY. 2005. Gate-refreshable nanowire chemical sensors. *Appl. Phys. Lett.* 86:123510
63. Wang C, Li ZY, Zhang HN, Zheng W, Wang W, et al. 2008. Highly sensitive and stable humidity nanosensors based on LiCl doped TiO_2 electrospun nanofibers. *J. Am. Chem. Soc.* 130:5036–37
64. Francioso L, Taurino AM, Forleo A, Siciliano P. 2008. TiO_2 nanowires array fabrication and gas sensing properties. *Sens. Actuators B Chem.* 130:70–76
65. Rothschild A, Kim ID, Lee BH, Kim DY, Jo SM, Tuller HL. 2006. Ultrasensitive chemiresistors based on electrospun TiO_2 nanofibers. *Nano Lett.* 6:2009–13
66. Joshi RK, Hu Q, Am F, Joshi N, Kumar A. 2009. Au decorated zinc oxide nanowires for CO sensing. *J. Phys. Chem. C* 113:16199–202
67. Ahn MW, Park KS, Heo JH, Park JG, Kim DW, et al. 2008. Gas sensing properties of defect-controlled ZnO-nanowire gas sensor. *Appl. Phys. Lett.* 93:263103
68. Law JBK, Thong JTL. 2008. Improving the NH_3 gas sensitivity of ZnO nanowire sensors by reducing the carrier concentration. *Nanotechnology* 19:205502
69. Yong KJ, Kwak G. 2008. Adsorption and reaction of ethanol on ZnO nanowires. *J. Phys. Chem. C* 112:3036–41
70. Wu JM. 2010. A room temperature ethanol sensor made from *p*-type Sb-doped SnO_2 nanowires. *Nanotechnology* 21:235501
71. Lin YR, Hsueh TJ, Chang SJ, Hsu CL, Chen IC. 2007. Highly sensitive ZnO nanowire ethanol sensor with Pd adsorption. *Appl. Phys. Lett.* 91:053111
72. Hwang IS, Choi JK, Woo HS, Kim SJ, Jung SY, et al. 2011. Facile control of C_2H_5OH sensing characteristics by decorating discrete Ag nanoclusters on SnO_2 nanowire networks. *Am. Chem. Soc. Appl. Mater. Interfaces* 3:3140–45
73. Morin FJ. 1959. Oxides which show a metal-to-insulator transition at the Neel temperature. *Phys. Rev. Lett.* 3:34–36
74. Stefanovich G, Pergament A, Stefanovich D. 2000. Electrical switching and Mott transition in VO_2. *J. Phys. Condens. Matter* 12:8837–45
75. Kolmakov A, Strelcov E, Lilach Y. 2009. Gas sensor based on metal-insulator transition in VO_2 nanowire thermistor. *Nano Lett.* 9:2322–26
76. Mai LQ, Xu L, Gao QA, Han CH, Hu B, Pi YQ. 2010. Single β-$AgVO_3$ nanowire H_2S sensor. *Nano Lett.* 10:2604–8
77. Lewis FA. 1967. *The Palladium Hydrogen System*. London/New York: Academic. 178 pp.
78. Penner RM, Walter EC, Favier F. 2002. Palladium mesowire arrays for fast hydrogen sensors and hydrogen-actuated switches. *Anal. Chem.* 74:1546–53
79. Hughes RC, Schubert WT, Buss RJ. 1995. Solid-state hydrogen sensors using palladium-nickel alloys—effect of alloy composition on sensor response. *J. Electrochem. Soc.* 142:249–54
80. Hughes RC, Schubert WK. 1992. Thin films of Pd/Ni alloys for detection of high hydrogen concentrations. *J. Appl. Phys.* 71:542–44

81. Dasari R, Zamborini FP. 2008. Hydrogen switches and sensors fabricated by combining electropolymerization and Pd electrodeposition at microgap electrodes. *J. Am. Chem. Soc.* 130:16138–39
82. Kiefer T, Villanueva LG, Fargier F, Favier F, Brugger J. 2010. The transition in hydrogen sensing behavior in noncontinuous palladium films. *Appl. Phys. Lett.* 97:121911
83. Kiefer T, Villanueva LG, Fargier F, Favier F, Brugger J. 2010. Fast and robust hydrogen sensors based on discontinuous palladium films on polyimide, fabricated on a wafer scale. *Nanotechnology* 21:505501
84. Xu T, Zach MP, Xiao ZL, Rosenmann D, Welp U, et al. 2005. Self-assembled monolayer-enhanced hydrogen sensing with ultrathin palladium films. *Appl. Phys. Lett.* 86:203104
85. Penner RM, Kaltenpoth G, Schnabel P, Menke E, Walter EC, Grunze M. 2003. Multimode detection of hydrogen gas using palladium-covered silicon μ-channels. *Anal. Chem.* 75:4756–65
86. Offermans P, Tong HD, van Rijn CJM, Merken P, Brongersma SH, Crego-Calama M. 2009. Ultralow-power hydrogen sensing with single palladium nanowires. *Appl. Phys. Lett.* 94:223110
87. Xiao ZL, Zeng XQ, Latimer ML, Panuganti S, Welp U, et al. 2011. Hydrogen gas sensing with networks of ultrasmall palladium nanowires formed on filtration membranes. *Nano Lett.* 11:262–68
88. Penner RM, Yang F, Taggart DK. 2010. Joule heating a palladium nanowire sensor for accelerated response and recovery to hydrogen gas. *Small* 6:1422–29
89. Penner RM, Yang F, Kung SC, Cheng M, Hemminger JC. 2010. Smaller is faster and more sensitive: the effect of wire size on the detection of hydrogen by single palladium nanowires. *Am. Chem. Soc. Nano* 4:5233–44
90. Penner RM, Yang F, Taggart DK. 2009. Fast, sensitive hydrogen gas detection using single palladium nanowires that resist fracture. *Nano Lett.* 9:2177–82
91. Myung NV, Hangarter CM, Bangar M, Mulchandani A. 2010. Conducting polymer nanowires for chemiresistive and FET-based bio/chemical sensors. *J. Mater. Chem.* 20:3131–40
92. Kaner RB, Li D, Huang JX. 2009. Polyaniline nanofibers: a unique polymer nanostructure for versatile applications. *Acc. Chem. Res.* 42:135–45
93. Weiller BH, Huang JX, Virji S, Kaner RB. 2003. Polyaniline nanofibers: facile synthesis and chemical sensors. *J. Am. Chem. Soc.* 125:314–15
94. Kaner RB, Huang JX. 2004. A general chemical route to polyaniline nanofibers. *J. Am. Chem. Soc.* 126:851–55
95. Kaner RB, Huang JX. 2004. Nanofiber formation in the chemical polymerization of aniline: a mechanistic study. *Angew. Chem. Int. Ed.* 43:5817–21
96. Doshi J, Reneker DH. 1995. Electrospinning process and applications of electrospun fibers. *J. Electrost.* 35:151–60
97. Reneker DH, Chun I. 1996. Nanometre diameter fibres of polymer, produced by electrospinning. *Nanotechnology* 7:216–23
98. Xia YN, Li D, Wang YL. 2003. Electrospinning of polymeric and ceramic nanofibers as uniaxially aligned arrays. *Nano Lett.* 3:1167–71
99. Xia YN, Li D. 2004. Electrospinning of nanofibers: reinventing the wheel? *Adv. Mater.* 16:1151–70
100. Kaner RB, Virji S, Huang JX, Weiller BH. 2004. Polyaniline nanofiber gas sensors: examination of response mechanisms. *Nano Lett.* 4:491–96
101. Craighead HG, Liu HQ, Kameoka J, Czaplewski DA. 2004. Polymeric nanowire chemical sensor. *Nano Lett.* 4:671–75
102. Myung NV, Chartuprayoon N, Hangarter CM, Rheem Y, Jung H. 2010. Wafer-scale fabrication of single polypyrrole nanoribbon–based ammonia sensor. *J. Phys. Chem. C* 114:11103–8
103. Weiller BH, Fowler JD, Virji S, Kaner RB. 2009. Hydrogen detection by polyaniline nanofibers on gold and platinum electrodes. *J. Phys. Chem. C* 113:6444–49
104. Weiller BH, Virji S, Kaner RB. 2006. Hydrogen sensors based on conductivity changes in polyaniline nanofibers. *J. Phys. Chem. B* 110:22266–70
105. Gu F, Shang L, Yin X, Tong L. 2008. Polymer single-nanowire optical sensors. *Nano Lett.* 8:2757–61

Annual Review of
Analytical Chemistry

Volume 5, 2012

Contents